In-Channel Experiments on Vertical Swimming with Bacteria-Like Robots

Ahmet Fatih Tabak, *Member, IEEE*, Serhat Yesilyurt, *Member, IEEE*

***Abstract*— Bio-inspired micro-robots are of great importance as to implement versatile microsystems for a variety of in *vivo* and in *vitro* applications in medicine and biology. Accurate models are necessary to understand the swimming and rigid-body dynamics of such systems. In this study, a series of experiments are conducted with a two-link cm-scale bio-inspired robot moving vertically without a tether, in silicone-filled narrow cylindrical glass channels. Swimming velocities are obtained for a set of varying tail and wave geometries, and employed to validate a resistive force theory (RFT) model using modified resistance coefficients based on measured forward velocity and body rotation rates.**

I. Introduction

Microsystems and micro-robotic devices are considered as tools of special therapeutic operations in the future [1]-[3]. Several experiments with bio-inspired artificial micro-swimmers are conducted to study the controlled swimming motion [4]-[5]; however, studies are greatly restricted with the power transfer in living tissue and micro manufacturing facilities. On the other hand, microsystems actuated by bacteria present a new type of cybernetic system and an alternative solution to the energy supply problem in micro- and nano-dimensions [6]-[7]. One possible application is using the controlled motion of bacteria species for micro positioning with high precision. Moreover, it is stated that natural micro-swimmers such as some bacteria species present controllable means of actuation in micro-dimensions [8]-[9].

It is demonstrated that certain bacteria can directly be integrated in computer controlled cybernetic microsystems in micro-scale applications [10]-[13]. Experiments with selected species show that it is possible to control the velocity by directly intervening with the rotation rate of the bacterial motor [10]-[11], or a bacterium can be maneuvered to carry out specific tasks by real-time computer control [12]-[13]. It is necessary to understand the swimming dynamics of single celled organisms to achieve accurate trajectory control in three-dimensions; to that end, the need for further study on bacterial swimming is clearly indicated.

There are some studies to manufacture rotary motors [14] to simulate bacterial motors [15]. Furthermore, untethered swimming experiments with artificial rotary motors in micro-scale are not reported to our knowledge; however, macro-scale experiments with dedicated DC-motors are conducted to mimic the bacterial swimming conditions [16]-[17]. Chen *et al.* [16] studied the motion of a bacteria-like robot with four helical tails placed symmetrically and actuated by DC-motors controlled individually. Authors demonstrated the 6-dof maneuverability of the robot in a viscous reservoir by separately controlling the rotation rate of each tail. Tabak and Yesilyurt [17]-[18] studied the horizontal swimming of a bacteria-like robot in narrow cylindrical channels. Authors demonstrated the effect of channel diameter on swimming velocities and presented a discussion on the importance of surface friction in in-channel swimming. Analytical models are developed to predict the swimming velocities of such robotic prototypes.

There are two distinct analytical approaches to predict the velocity of a micro-scale swimmer comprised of a body and a tail: slender body theory and resistive force theory. Slender body theory (SBT) is based on singularities signified by Stokeslet functions representing the induced flow fields around a moving slender rod [19]-[20]. Resistive force theory (RFT) assumes creeping motion in still viscous fluids and calculates the hydrodynamic resistance acting per unit length along a slender rod [21]-[22]. RFT method predicts the swimming velocities much faster; however, SBT method proves to be more accurate [23]-[24]. This issue can be addressed by simply modifying the resistance coefficients of the body of the swimmer [25].

In this study we conducted experiments on vertical in-channel swimming of bio-inspired robots in order to collect swimming data to be used in validation of numerical models. The robot comprises of two links, i.e. body and tail, capable of rotating in opposite directions: body contains the driving system which actuates the tail. The body is designed to be neutrally buoyant hence the swimmer moves upwards without touching the surfaces of the channel. Motion of the robot is captured by a CCD-camera and swimming velocities are measured by frame-by-frame investigation. Parameterized geometry study is carried out to obtain swimming velocities for varying wave length, wave amplitude and tail length. A reduced-order analytical model based on resistive force theory (RFT) with modified resistance matrix is implemented to predict the swimming

Research supported in part by The Scientific and Technological Research Council of Turkey.

A. F. Tabak was a Ph.D. candidate with the Department of Mechatronics Engineering, Faculty of Engineering and Natural Sciences, Sabanci University, 34956 Istanbul Turkey. He is now with the Department of Mechatronics Engineering, Faculty of Engineering and Design, Istanbul Commerce University, 34840 Istanbul Turkey. (e-mail: aftabak@ticaret.edu.tr).

S. Yesilyurt is with the Department of Mechatronics Engineering, Faculty of Engineering and Natural Sciences, Sabanci University, 34956 Istanbul Turkey. (e-mail: syesilyurt@sabanciuniv.edu).

velocities. It is demonstrated that the numerical model results agree well with the observed data.

II. Methodology

A. Bio-Inspired Robot and Experimental Setup

Fig. 1(a) demonstrates the inner structure of the bio-mimetic robot. Robot is comprised of two rigid-links, i.e. body and tail, which are hold together with a revolute joint and free to rotate in opposite direction as some bacterium species with single flagellum exhibit [24]. Fig. 1(b) illustrates the experimental setup which consists of a glass tube filled with silicone oil, a CCD-camera, and the robot itself.

Body constitutes the payload which includes a dedicated coreless brushed DC-motor with enough torque to overcome the viscous forces acting on the tail and push the entire swimmer forward. The DC-motor is controlled by a driving circuitry generating a PWM signal at high frequency. The tail rotation is triggered by a remote controller to which an embedded IR-receiver is responsible for on-off actuation. The driving system is powered by a rechargeable Li-Po battery pack which capable of sustaining continuous operation for approximately 10 minutes. The battery is recharged for each individual experiment. Electrochemical and electromechanical components are sealed in a casing made out of silica glass, which is 18 mm in diameter.

At the tip of the casing, a cylindrical cork 20 mm in diameter is glued to assure neutral buoyancy along the **Z**-axis in the lab frame: the restoring-torque due to the buoyancy force acting on the cork restricts rigid-body rotations of the swimmer holding it steadily in upwards direction, thus eliminating collusions with the channel walls due to rigid body rotation in directions perpendicular to the axis of the channel. Hence, the friction and lubrication problems encountered during previous studies are avoided [17]-[18].

On the bottom of the casing there is a plastic sealing element 20 mm in diameter, which holds the DC-motor whose rotor sticks out the body and inserted into the mechanical coupler. The rotor, in effect, constitutes the revolute joint which allows body and tail to rotate in opposite directions. The details of the bio-inspired robot are given in Table I.

The second link to the robot is the tail which is manufactured out of copper wire, 1 mm in diameter: the wire is coiled around a cylindrical object of constant diameter and stretched uniformly until a certain wave length and wave amplitude is obtained throughout the helix. To ensure that the average density of the robot is equal to that of the silicone oil, the cord length ℓ of the tail is kept fixed; however, the apparent length of the helix differs. Six different tail geometries are used in the experiments to study the effect of wave length λ, wave amplitude B_o, tail length L_t, and actuation frequency f. The latter is not a controlled parameter; however, differs as the tail geometry varies. Wave and tail dimensions with corresponding actuation frequencies are presented in Table II.

Fig 2(a) depicts the robot placed in a glass tube filled with silicone oil, which has a dynamic viscosity approximately 3500 times that of the water in room temperature, which is obtained as a mixture of 12.5 Pa·s and 1 Pa·s with a certain ratio. The silicone oil is used because its sensitivity is minimal to temperature variations during experiments. The channel is placed in vertical position such that the robot would swim opposite to the gravitational pull. Both ends of the channel are sealed so that the bio-inspired robot is operating fully submerged in a confined viscous medium.

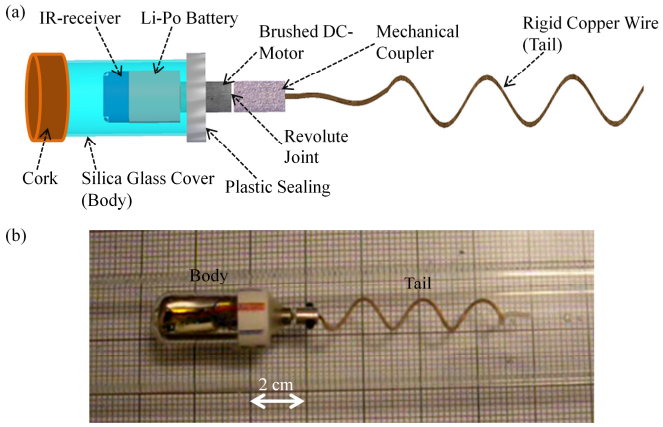

Fig. 1. Bio-inspired robot: (a) design with the links and driving elements; (b) picture of the manufactured prototype in horizontal glass channel.

TABLE I PHYSICAL PROPERTIES OF BIOMIMETIC ROBOT AND EXPERIMENTAL SETUP

D_{ch}	Channel Diameter	35 mm
L_{ch}	Channel Length	350 mm
D_b	Overall Body Diameter	20 mm
L_b	Total Body Length	50 mm
D_c	Coupler Diameter	6 mm
L_c	Coupler Length	10 mm
D_t	Copper Wire Diameter	1 mm
-	Total Body Mass	11 g
-	DC-motor Diameter	6 mm
-	DC-motor Length	11 mm
-	Rotor Diameter	0.8 mm
-	Li-Po Battery Volume	5.5 mm x14mm x17mm
-	Li-Po Battery Rating	70 mA·h with 3.7 V
ρ	Si-Oil Density	985 kg/m^3
μ	Si-Oil Viscosity	3.5 Pa·s
-	CCD-Camera	640-by-480 Pixels @ 30 fps
-	CCD-Camera Distance	150 mm

TABLE II. TAIL AND WAVE GEOMETRIES

Tail	λ (mm)	B_o (mm)	L_t (mm)	f [1] (Hz)
#1	15.5	2.50	130.0	1.05
#2	10.0	2.50	88.0	1.50
#3	16.0	4.50	93.0	0.94
#4	12.0	4.50	60.0	0.91
#5	15.0	7.50	56.0	0.57
#6	11.0	7.50	42.0	0.57

[1] Observed

The CCD-camera which is capable of capturing images at 30 fps is placed 15 cm away from the glass channel assuring a fixed region of interest such that swimming is captured at the same location of the channel (see Fig 2(b)). Experiments are recorded with the CCD-camera and consecutive frames are studied to calculate the average swimming velocities between a certain pair of marks placed on the channel surface. The errors in observation due to the spatial resolution of the CCD-camera are averaged out by repetitive experiments. Further details of the experimental setup are also available in Table I.

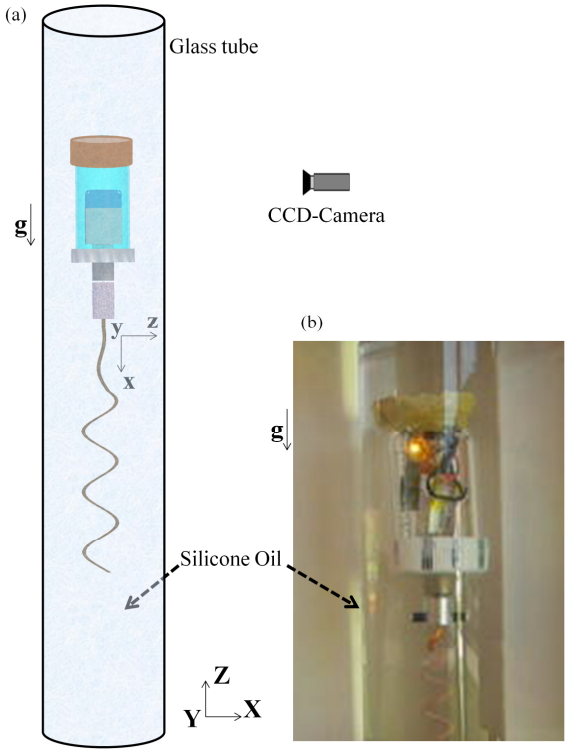

Fig. 2. Experimental setup: (a) design of the experimental setup with the robot inside a glass channel and a CCD-camera placed in front; (b) a representative scene captured by the CCD-camera.

B. Resistive Force Theory (RFT) Model

Trajectory of a two-link bio-inspired robot submerged in low Reynolds number flows is governed by the equation of motion by which all rigid-body accelerations are omitted and the hydrodynamic forces are determined based on linear resistance approximation of RFT method:

$$\mathcal{F}_{\mathrm{b}} + \mathcal{F}_{\mathrm{t}} + \mathcal{F}_{back\text{-}flow} = 0, \tag{1}$$

$$\mathcal{F}_{\mathrm{b,t}} = -\mathbf{B}_{\mathrm{b,t}}\mathbf{V}_{\mathrm{b,t}}, \tag{2}$$

where $\mathcal{F}$ is the six-by-one generalized force-torque vector, subscripts b and t denote body and tail of the robot, respectively. Here, $\mathbf{V}$ is the generalized six-by-one rigid-body velocity vector, and $\mathbf{B}$ is the six-by-six hydrodynamic resistance matrix. Furthermore, given the fact that both ends of the channel are sealed, a back-flow is induced by the replaced fluid due to the rigid-body translation of the bio-inspired robot: the subscript '*back-flow*' denotes the hydrodynamic drag exerted on the body by that flow.

Given the position vector on the right-handed rotating helix is specified with $\mathbf{P}$ and the rotation rate of the tail is $\omega = 2\pi f$, the rotational velocity vector on the surface of helix is signified as $\mathrm{d}\mathbf{P}/\mathrm{d}t = \boldsymbol{\Omega}_{\mathrm{t}} \times \mathbf{P}$, where t denotes time and the tail rotation rate vector is $\boldsymbol{\Omega}_{\mathrm{t}} = [\omega \ 0 \ 0]^T$, and superscript T signifying the transpose.

Hydrodynamic resistance matrix for the tail is calculated from the integration of the local force coefficients projected onto the swimmer coordinates from the local Frenet-Serret [26] frames on the tail in the following fashion:

$$\mathbf{B}_{\mathrm{t}} = \int_{\mathrm{L_t}} \begin{bmatrix} \mathbf{R}\,\mathbf{C}\,\mathbf{R}^T & -\mathbf{R}\mathbf{C}\,\mathbf{R}^T\mathbf{S} \\ \mathbf{S}\,\mathbf{R}\,\mathbf{C}\,\mathbf{R}^T & -\mathbf{S}\,\mathbf{R}\,\mathbf{C}\,\mathbf{R}^T\mathbf{S} \end{bmatrix} (\ell / \mathrm{L_t})\, \mathrm{d}x \tag{3}$$

Here, $\mathbf{S}$ is the skew-symmetric matrix corresponding to the local cross product. $\mathbf{R}$ signifies the rotation matrix between the local **tnb**-frame, i.e. with local tangential, normal and bi-normal directions, and the swimmer frame as depicted in Fig. 3.

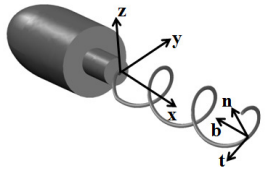

Fig. 3. Local Frenet-Serret frames (**tnb**) and swimmer frame (**xyz**).

The local hydrodynamic resistance acting on the tail is signified by the matrix $\mathbf{C}$ in (3), which consists of the local resistance coefficients in the tangent, bi-normal, and normal directions. Gray and Hancock [21] articulate a resistive coefficient set based on RFT method as:

$$c_t = 2\pi\mu \Big/ \left(\log\left(\lambda / \mathrm{D_t}\right) - 0.5\right) \tag{4}$$

in tangential direction, and

$$c_{n,b} = 4\pi\mu \Big/ \left(\log\left(\lambda / \mathrm{D_t}\right) + 0.5\right) \tag{5}$$

in normal and bi-normal directions, respectively. Moreover, Lighthill [20] formulated a sub-optimal resistive coefficient set based on the SBT method:

$$c_t = 2\pi\mu / \log\left(0.36\lambda / \alpha \mathrm{D_t}\right) \tag{6}$$

in tangential direction, and

$$c_{n,b} = 4\pi\mu \Big/ \left(\log\left(0.36\lambda / \alpha \mathrm{D_t}\right) + 0.5\right) \tag{7}$$

in normal and bi-normal directions, respectively, where α is ratio of apparent tail length to the actual chord length, i.e $\alpha = \mathrm{L_t}/\ell$.

The drag force acting on the body due to the back-flow of the replaced silicone oil is calculated as follows [27]:

$$\mathcal{F}_{back-flow} = -\mathbf{B}_{\mathrm{b}} \begin{bmatrix} \mathbf{U}_{back-flow} \\ \mathbf{0} \end{bmatrix} \tag{8}$$

Here, the average velocity of the back-flow around the body of the swimmer is calculated as:

$$\mathbf{U}_{back-flow} = \begin{bmatrix} -U_{robot} \dfrac{R_{body}^2}{R_{ch}^2 - R_{body}^2} & 0 & 0 \end{bmatrix}^T \tag{9}$$

where U_{robot} is the observed swimming velocity in **x**-direction in the swimmer's frame of reference, R_{ch} and R_{body} signify the channel radius and the radius on the short axis of the body, respectively. The resistance matrix of the rigid body in (8) is generalized as follows:

$$\mathbf{B}_{\mathrm{b}} = \begin{bmatrix} \mathbf{D} & \mathbf{G} \\ \mathbf{G}^T & \mathbf{E} \end{bmatrix} \tag{10}$$

where **D** and **E** are assumed to be 3×3 diagonal coefficient matrices corresponding to translational and rotational hydrodynamic resistances acting on the body, and the matrix **G** is considered zero for an axisymmetric body with its center of geometry rests on the long axis of the bio-inspired robot. The non-uniform shape of the body studied in this text calls for a modified resistance coefficient set which accounts for the geometric aberrations and channel effects [28], [29], [30]. The coefficients used in this study are given by [28] with suitable amplitude corrections; $\Upsilon_{T,x}$ and $\Upsilon_{R,x}$, for rigid-body translations and rotations along **x**-direction, respectively, as $D_x = \Upsilon_{T,x}\mathbf{D}(1,1)$ and $E_x = \Upsilon_{R,x}\mathbf{E}(1,1)$. The actuation system is not included in this study given the fact that work done by the DC-motor is assumed to be entirely against viscous forces and torques acting on rotating surfaces.

From the equation of motion one obtains the swimming velocities of the bio-inspired robot as follows:

$$\begin{bmatrix} \mathbf{U}_{robot} \\ \boldsymbol{\Omega}_{\mathrm{b}} \end{bmatrix} = -\left(\mathbf{B}_{\mathrm{b}} + \overline{\mathbf{B}}_{\mathrm{t}}\right)^{-1} \left(\mathbf{B}_{\mathrm{t}} \begin{bmatrix} \mathbf{0} \\ \boldsymbol{\Omega}_{\mathrm{t}} \end{bmatrix} - \mathcal{F}_{back-flow} \right) \tag{11}$$

where $\overline{\mathbf{B}}_{\mathrm{t}}$ is the modified tail resistance matrix: it is necessary to set the fourth column and the fourth row of the hydrodynamic resistance matrix of the tail to zero given that the **x**-rotation of the helix is specified as the tail actuation frequency [30], which is obtained via observations. It is also noted that, one may restrict the motion in an arbitrary direction by setting corresponding rows and columns of the resistance matrices to zero. In this study all lateral rigid-body rotations are eliminated in order to simulate the conditions in the experiment.

III. Results

Swimming velocities are calculated averaging out results obtained from five distinct observations. Resolution of the captured images and the frame-rate of the CCD-camera are apt to resolve the body and tail rotation rates and the forward translation of the robot. Observed rotation rates of the tail are used as actuation frequency in the RFT model, and the computed velocity values are compared against the observations in dimensionless form, i.e. with the ratio of **x**-velocities as U_{robot}/U_{wave} with $U_{wave} = \lambda f$ and $\Omega_{body}/\omega_{tail}$ to eliminate the effects of actuation frequency f, as presented in Fig 4. Numerical predictions are acquired by averaging out two complete periods of tail rotation. Provided that the forward velocity component is dominant in rigid-body translations, for sake of simplicity, we cast the RFT model for motion along the **x**-direction only. The helical tail is discretized with 100 nodes per wavelength. Integration in the time-domain is carried out by non-stiff Runge-Kutta solver [31]. The amplitude corrections to the body resistances, which are needed to predict the swimming velocities within overall 10% error for the ratio of $B_o/R_{body} = 0.45$, are given in Table III. It is noted that above corrections are implemented and used for each RFT calculation. Moreover, the observed velocities with 95% confidence intervals are presented in Table IV. It is also noted that the highest calculated Reynolds number with body diameter being the characteristic length is roughly 0.0033, thus creeping flow assumptions and RFT approach are valid.

TABLE III. Corrections to The Body Resistance

RFC Set	Corrections
Sir Lighthill [19]	$\{\Upsilon_{T,x} = 4.5,\ \Upsilon_{R,x} = 3.4\}$
Gray and Hancock [20]	$\{\Upsilon_{T,x} = 16,\ \Upsilon_{R,x} = 1.4\}$

TABLE IV. Observed Averaged-out Swimming Velocities with Confidence Intervals

Tail	U_{robot} (mm/s)	95%(mm/s)	Ω_b (Hz)	95%(Hz)
#1	0.5860	0.0640	0.0998	0.0006
#2	0.2208	0.0051	0.1183	0.0009
#3	0.2736	0.0041	0.1283	0.0002
#4	0.2609	0.0040	0.1299	0.0004
#5	0.3950	0.0119	0.1449	0.0001
#6	0.2171	0.0045	0.1403	0.0001

Table IV indicates that as the wave amplitude increases the forward velocity increases; however, with two exceptions, i.e. tail #1 and #6 being the fastest and the lowest body-tail combinations, respectively (see Table II). Similarly, increasing wave amplitudes result in amplified body rotation rates. Furthermore, Table IV demonstrates that as the total number of waves increases, the forward velocity decreases with increasing body rotation rates; however, with one exception, i.e. tail #6 (see Table II). Nonetheless, further study with dimensionless velocities is required to be able to ascertain the effect of total number of waves and wave amplitude without the effect of actuation frequency of the tail.

Dimensionless velocity results indicate that the U_{robot}/U_{wave} ratio decreases in magnitude nonlinearly with increasing total number of waves N_λ, i.e. with decreasing wave length for fixed chord length as depicted in Fig. 4(a)

and Fig. 4(c), with an exception for B_o/R_{body} = 0.45 where the change in velocity ratio is less than 1% as shown in Fig. 4(b). In effect, the thrust generated by the rotating helical tail drops with increasing N_λ and decreasing α, i.e. as the helix converges to a hollow cylinder and hydrodynamic resistance increases along **x**-direction in the swimmer's frame and also along **Z**-direction in the lab frame. Furthermore, the $\Omega_{body}/\omega_{tail}$ ratio slightly decreases in magnitude with increasing N_λ as depicted in Fig. 4(d) and Fig. 4(f). It is noted that, similar to the forward velocity results, the change in ratio is minimal for B_o/R_{body} = 0.45 (see Fig. 4(e)).

Parameterized wave amplitude results show that the U_{robot}/U_{wave} ratio slightly increases in magnitude with increasing B_o (see Figs. 4(a)-(c)), with a single exception for tail #1 (see Table II): the significant jump in forward velocity depicted in Fig 4(a) indicates extra thrust generated based on lubrication between the tail and channel walls. It is noted that maintaining coaxial swimming is unrealistic with comparable channel and tail lengths.

Lastly, the $\Omega_{body}/\omega_{tail}$ ratio tends to increase in magnitude with increasing B_o: as the helix diameter increases, the hydrodynamic resistance to its rotation also increases leading to higher body rotation rates provided that the torque output of the DC-motor is constant during each individual experiment.

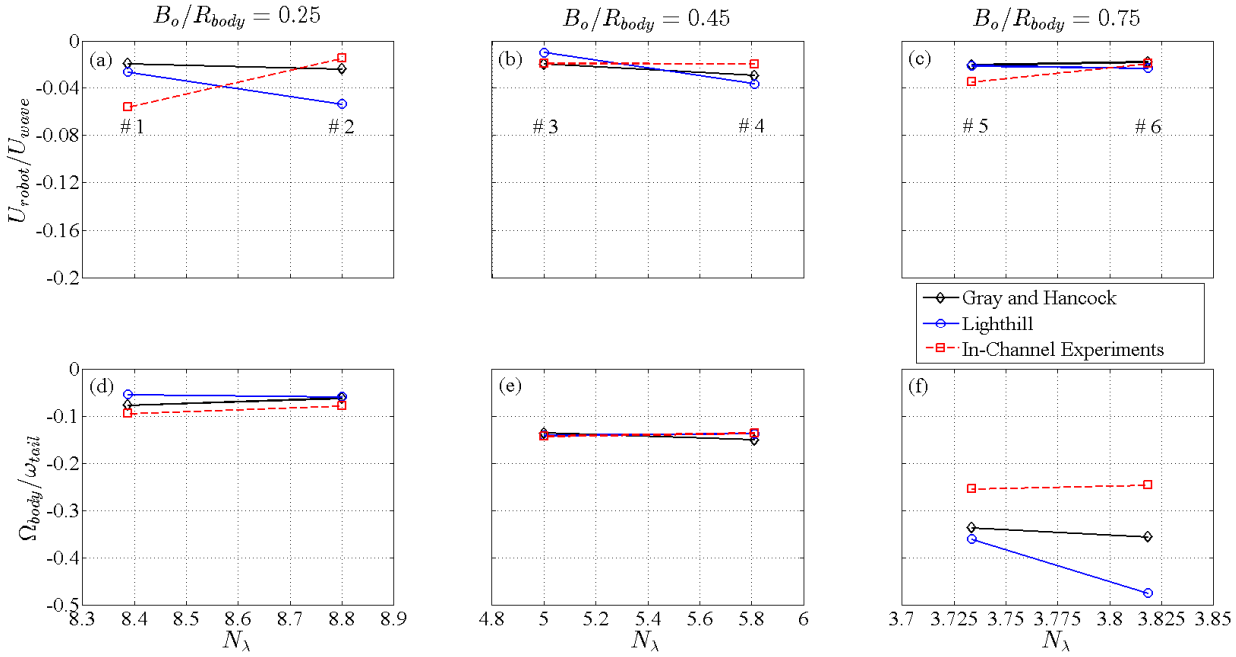

Fig. 4. Vertical channel observations (red) predicted with resistive force coefficients presented by Lighthill [20] (blue) and Gray and Hancock [21] (black): (a)-(b) dimensionless forward velocity results; (d)-(f) dimensionless rotation rate results.

The RFT model predictions agree well with the observed forward velocities for high wave amplitudes with a single correction on body resistance. However, as the wave amplitude decreases further calibration is required to obtain accurate results. Force coefficient set articulated by Gray and Hancock [21] are slightly superior to the set given by Lighthill [20]. On the other hand, RFT model predicts the body rotation rates with higher accuracy for smaller wave amplitudes; but, predictions fail as the B_o/R_{body} ratio reaches to 0.75. It is noted that, the force coefficients presented by Gray and Hancock perform slightly better for small wave amplitudes, whereas RFT model with the single resistance calibration produce incorrect results as to predict the body rotation rates for larger wave amplitudes with both coefficient set.

IV. Conclusion

In this study a bio-inspired two-link robot is built with a revolute joint allowing the links, i.e. body and tail, rotate in opposite directions along the long axis as some bacterium species exhibit. Body of the swimmer carries an on-board power supply and remote control circuitry; hence the swimming motion is obtained without a tether.

The bio-inspired robot is placed inside a circular glass channel, which is positioned parallel to the gravitational attraction. The channel is filled with a high viscosity silicone oil to ensure Re < 0.1 condition; hence satisfying creeping flow assumptions.

A cylindrical piece of cork is glued at the tip of the body to ensure neutral buoyancy for rigid-body motions along the **x**-direction in the swimmer frame: the restoring-torque applied by the cork restricts rigid-body rotations of the bio-inspired swimmer along lateral direction thus forcing the swimmer follow the symmetry axis of the channel in concentric form along the **Z**-axis in the lab frame. Horizontal experiments without surface contact or invoking lubrication effects are simply hard to conduct due to the fact that achieving neutral buoyancy in lateral axes of the bio-inspired swimmer is a demanding task.

Six different rigid helical tails with parameterized wave geometries are manufactured and employed individually. In-channel swimming in vertical direction is captured by a capable CCD-camera and the resolution error is averaged out by repetitive experiments: each body-tail combination is tested for a total of five times and observed velocities are averaged with confidence intervals.

Experimental results are used for validation of analytical and numerical models [32]. Furthermore, observed tail rotation rates are imposed as actuation frequencies and the calculated swimming velocities are compared with experiments. The irregular body shape is compensated with a single numerical calibration on the hydrodynamic resistance matrix, and the extra fluid drag due to the back-flow induced by the rigid-body translation of the bio-inspired robot inside the cylindrical closed channel is also included in the RFT model.

Calculations are in good agreement with experimental results except that the forward velocity predictions fail with small wave amplitudes and body rotation rate predictions fail with large wave amplitudes. The overall performance of the RFT model is reasonably well and the resistive force coefficient set given by Gray and Hancock [21] performs slightly better with a single resistance calibration. Furthermore, the restoring-torque exerted on the swimmer restricted the lateral rigid-body rotations and avoided the complications due to surface friction with lubrication phenomenon, which lets omission of DC-motor equations [18] altogether thus simplifying the model and the analysis.

It is noted that one may obtain less than 0.1% prediction error for all six cases by applying six separate calibrations; however, such an approach would hinder the efforts to inspect the time-averaged performance of the RFT model with parameterized wave and tail geometries.

REFERENCES

[1] S. Martel, "Collective methods of propulsion and steering for untethered microscale nanorobots navigating in the human vascular network," *Proc. Inst. Mech. Eng. Pt. C J. Mechan. Eng. Sci.*, vol. 224, pp. 1505-1513, Jul. 2010.

[2] B. J. Nelson, I. K. Kaliakatsos, and J. J. Abbott, "Microrobots for minimally invasive medicine," *Annu. Rev. Biomed. Eng.,* vol. 12, pp. 55-85, Apr. 2010.

[3] R. Bogue, "The development of medical microrobots: a Review of progress," *Ind. Robot*, vol. 35, No. 4, pp. 294-299, 2008.

[4] R. Dreyfus, J. Baudry, M. L. Roper, M. Fermigier, H. A. Stone, J. Bibette, "Microscopic artificial swimmers," *Nature*, vol. 437, pp. 862-865, Oct. 2005.

[5] L. Zhang, J. J. Abbot, L. Dong, B. E. Kratochvil, D. Bell, B. J. Nelson, "Artificial bacterial flagella: fabrication and magnetic control," *Appl. Phys. Lett.*, vol. 94, iss. 6, 064107, 2009.

[6] X. Xiong, M. E. Lidstrom, B. A. Parviz, "Microorganisms for MEMS," *J. Microelectromech. S.*, vol. 16, iss. 2, pp. 429-444, Apr. 2007.

[7] T. Fukuda, F. Arai, M. Nakajima, "Micro-Nanorobotic Manipulation Systems and Their Applications," ch. 5, pp. 137-139, Springer, Apr. 2013.

[8] S. Martel, "Bacterial microsystems and microrobots," *Biomed. Microdevices*, vol. 14, iss. 6, pp. 1033-1045, Dec. 2012.

[9] A. Sahari, D. Headen, B. Behkam, "Effect of body shape on the motile behavior of bacteria-powered swimming microrobots (BacteriaBots)," *Biomed. Microdevices*, vol. 14, iss. 6, pp. 999-1007, Dec. 2012.

[10] A. Uenoyama, M. Miyata, "Gliding ghosts of mycoplasma mobile," *P. Natl. Acad. Sci. USA*, vol. 102, no. 36, pp. 12754-12758, Sept. 2005.

[11] K. Nogawa, M. Kojima, M. Nakajima, S. Kojima, M. Homma, T. Fukuda, "Rotational speed control of Na^+-driven flagellar motor by nano/micro dual pipettes," *IEEE T. Nanobiosci.*, vol. 8, iss. 4, pp. 341-348, Dec. 2009.

[12] S. Martel, "Controlled bacterial micro-actuation," presented at the International Conference on Microtechnologies in Medicine and Biology, Okinawa, Japan, May 9-12, 2006.

[13] S. Martel, M. Mohammadi, "A robotic micro-assembly process inspired by the construction of the ancient pyramids and relying on several thousand flagellated bacteria acting as micro-workers," presented at The 2009 IEEE/RSJ International Conference on Intelligent Robots and Systems, St. Louis, USA, October 11-15, 2009.

[14] R. T. Tjeung, M. S. Hughes, L. Y. Yeo, J. R. Friend, "Surface acoustic wave micromotor with arbitrary axis rotational capability," *Appl. Phys. Lett.*, vol. 99, iss. 21, 214101, 2011.

[15] H. C. Berg, "The rotary motor of bacterial flagella," *Annu. Rev. Biochem.*, vol. 72, pp. 19-54, July 2003.

[16] B. Chen, S. Jiang, Y. Liu, Y. Yang, S. Chen, "Research on the kinematic properties of a sperm-like swimming micro robot," *J. Bionic Eng.*, vol. 7, pp. S123-S129, Sep. 2010.

[17] A. F. Tabak, S. Yesilyurt, "Experiments on in-channel swimming of an untethered biomimetic robot with different helical tails," presented at The 4th IEEE RAS/EMBS International Conference on Biomedical Robotics and Biomechatronics, Rome, Italy, June 24-27, 2012.

[18] A. F. Tabak, S. Yesilyurt, "Experiment-based kinematic validation of numeric modeling and control of an untethered biomimetic microrobot in channel," presented at The 12th IEEE International Workshop on Advanced Motion Control, Sarajevo, Bosnia and Herzegovina, Mar. 25-27, 2012.

[19] G. J. Hancock, "The self-propulsion of microscopic organisms through liquids," *P. Roy. Soc. Lond. A Mat.*, vol. 217, no. 1128, pp. 96-121, Mar. 1953.

[20] J. Lighthill, "Flagellar hydrodynamics: the John von Neumann lecture," *SIAM Rev.*, vol. 18, no. 2, pp. 161-230, Apr. 1976.

[21] J. Gray, G. J. Hancock, "The propulsion of sea-urchin spermatozoa," *J. Exp. Biol.*, vol. 32, pp. 802-814, Dec. 1955.

[22] C. Brennen, H. Winet, "Fluid mechanics of propulsion by cilia and flagella," *Annu. Rev. Fluid Mech.*, vol. 9, pp. 339-398, Jan. 1977.

[23] J. B. Keller, S. I. Rubinow, "Swimming of flagellated microorganisms," *Biophys. J.*, vol.16, iss. 2, pt. 1, pp. 151-170, Feb. 1976.

[24] S. Chattopadhyay, X.-L. Wu, "The effect of long-range hydrodynamic interaction on the swimming of a single bacterium," *Biophys. J.*, vol. 96, iss. 5, pp. 2023-2028, Mar. 2009.

[25] A. F. Tabak, F. Z. Temel, S. Yesilyurt, "Comparison on experimental and numerical results for helical swimmers inside channels," presented at The IEEE/RSJ Intelligent Robotics and Systems Conference, San Francisco CA, USA, Sept. 25-30, 2011.

[26] A. J. Hanson, H. Ma, "Quaternion frame approach to streamline visualization," *IEEE T. Vis. Comput. Gr.*, vol. 1, iss. 2, pp. 164-174, Jun. 1995.

[27] J. Happel, H. Brenner, "Low reynolds number hydrodynamics *with special applications to particulate media*," N.J.: Prentice-Hall, Inc., 1965, pp. 303.

[28] F. Perrin, "Mouvement brownien d'un ellipsoïde (I). Dispersion diélectrique pour des molecules ellipsoïdales," *J. Phys. Radium*, ser. 7, vol. 5, pp. 497-511, Oct. 1934.

[29] J. J. L. Higdon, G. P. Muldowney, "Resistance functions for spherical particles, droplets and bubbles in cylindrical channels," *J. Fluid Mech.*, vol. 298, no.1, pp. 193-210, Sept. 1995.

[30] A. F. Tabak, "Computational and microhydrodynamic modeling and experiments with bio-inspired swimming robots in cylindrical channels," Ph.D. dissertation, Department of Mechatronics Engineering, Sabanci University, Istanbul, 2012.

[31] L. F. Shampine, M. W. Reichelt, "The MATLAB ODE suite," *SIAM J. Sci. Comput.*, vol. 18, iss. 1, pp. 1–22, Jan. 1997.

[32] A. F. Tabak, S. Yesilyurt, "Improved kinematic models for two-link helical micro/nano-swimmers," *IEEE T. Robot.*, *Special Issue on Nanorobotics*, Mar. 2013. (submitted)